Regular Article

PLATELETS AND THROMBOPOIESIS

Q:A1

Myosin-II repression favors pre/proplatelets but shear activation generates platelets and fails in macrothrombocytopenia

Q:1 Kyle R. Spinler,[1] Jae-Won Shin,[1,2] Michele P. Lambert,[3,4] and Dennis E. Discher[1,2]

[1]Molecular & Cell Biophysics Laboratory and [2]Graduate Group in Pharmacological Science, University of Pennsylvania, Philadelphia, PA; [3]Divison of Hematology, The Children's Hospital of Philadelphia, Philadelphia, PA; and [4]Department of Pediatrics, Perelman School of Medicine at the University of Pennsylvania, Philadelphia, PA

Key Points

- Myosin-II inhibition (with blebbistatin) and *MYH9*-RD mutations enhance shear fragmentation to pre/proplatelet sizes.
- Sustained shear activates normal myosin-II, which then favors division of pre/proplatelets to smaller platelets.

Megakaryocyte ploidy and the generation of pre/proplatelets are both increased in culture by pharmacologic inhibition of myosin-II, but nonmuscle myosin-IIA (MIIA) mutations paradoxically cause *MYH9*-related diseases (*MYH9*-RD) that adversely affect platelets. In marrow, megakaryocytes extend projections into the microcirculation, where shear facilitates fragmentation to large pre/proplatelets, suggesting that fluid stresses and myosin-II activity somehow couple in platelet biogenesis. Here, in bulk shear, plateletlike particles generated from megakaryocytes are maximized at a shear stress typical of that in the microcirculation and after treatment with a myosin-II inhibitor. MIIA activity in static cells is naturally repressed through phosphorylation at Serine-1943, but shear decreases phosphorylation, consistent with MIIA activation and localization to platelet cortex. Micropipette aspiration of cells shows myosin-II accumulates at stressed sites, but its inhibition prevents such mechanoactivation and facilitates generation of CD41$^+$ fragments similar in size to pre/proplatelets. *MYH9*-RD mutants phenocopy inhibition, revealing a dominant negative effect. MIIA is diffuse in the large platelets of a *MYH9*-RD patient with macrothrombocytopenia and is also diffuse in normal pre/proplatelets treated with inhibitor that blocks in vitro division to small platelets. The findings explain the large platelets in *MYH9*-RD and the near-normal thrombocrit of patients. Myosin-II regulation thus controls platelet size and number. (*Blood*. 2014;00(00):1-9)

Introduction

Intravital imaging of mouse bone marrow[1] has shown that polyploid megakaryocytes (MKs) extend large and flexible proplatelet projections across the fenestrated endothelium into the bloodstream, where proplatelets are fragmented by fluid shear in minutes (Figure 1A),[2] but molecular mechanisms remain unclear. In vitro studies of mouse MKs have shown that proplatelet extensions can be increased ~two- to threefold in length with inhibition of nonmuscle myosin-II (MII) by the drug blebbistatin, which blocks the ATPase in the MII head region.[3,4] Treatment of human CD34$^+$–derived MKs with the same drug for 3 days increased both MK ploidy and proplatelet numbers, yielding up to fourfold more functional platelets in vitro and in vivo.[5] However, drug washout proved essential in the latter studies because normal platelets rely on MIIA to contract wounds and clots.[6,7] Myosin-II normally contributes to cytokinesis, membrane rigidity, and contraction of matrix, and so its transient inhibition explains both high ploidy MKs and increased proplatelets..[8] These pharmacologic findings and the fact that MIIA is expressed throughout hematopoiesis[9] lead us to hypothesize that normal MK-platelet physiology also involves an initial suppression of MIIA activity. This hypothesis brings into focus the cell function(s) that are dysregulated when MIIA (*MYH9*) is mutated in *MYH9*-related diseases (*MYH9*-RD). Patients who had previously been diagnosed with May-Hegglin anomaly, Epstein syndrome, or Fechtner syndrome all have autosomal-dominant *MYH9*-RD mutations,[10] with large platelets in reduced numbers (macrothrombocytopenia) and leukocyte inclusions at birth, as well as the progressive risks with age of the development of nephropathy, deafness, and/or cataracts.[11] Q:2

Myosin-II filament assembly is necessary for myosin-II contractility, but large inclusions suggest dysfunctional protein.[11-17] Nonetheless, mice with MK-specific MIIA knockout show a higher percentage of MKs with proplatelet buds and larger proplatelets, even though there are as much as 70% fewer platelets in peripheral blood.[14] Similar phenotypes are evident in mice expressing *MYH9*-RD mutations, such as D1424N, that occur in the filament-forming tail of MIIA.[18] The reason *MYH9*-RD mutants are not phenocopied by blebbistatin inhibition of myosin-II seems paradoxical, especially if our hypothesis is correct that normal MK-platelet physiology initially suppresses MIIA. Here we resolve this apparent paradox with evidence of transient suppression of MIIA in normal MKs that seems permanent in *MYH9*-RD mutants.

Materials and methods

Reagents, DNA constructs, cell lines, and standard methods are described in the supplemental Methods. All blood from patients and controls was

Submitted May 19, 2014; accepted November 5, 2014. Prepublished online as *Blood* First Edition paper, November 13, 2014; DOI 10.1182/blood-2014-05-576462.

The online version of the article contains a data supplement.

The publication costs of this article were defrayed in part by page charge payment. Therefore, and solely to indicate this fact, this article is hereby marked "advertisement" in accordance with 18 USC section 1734.

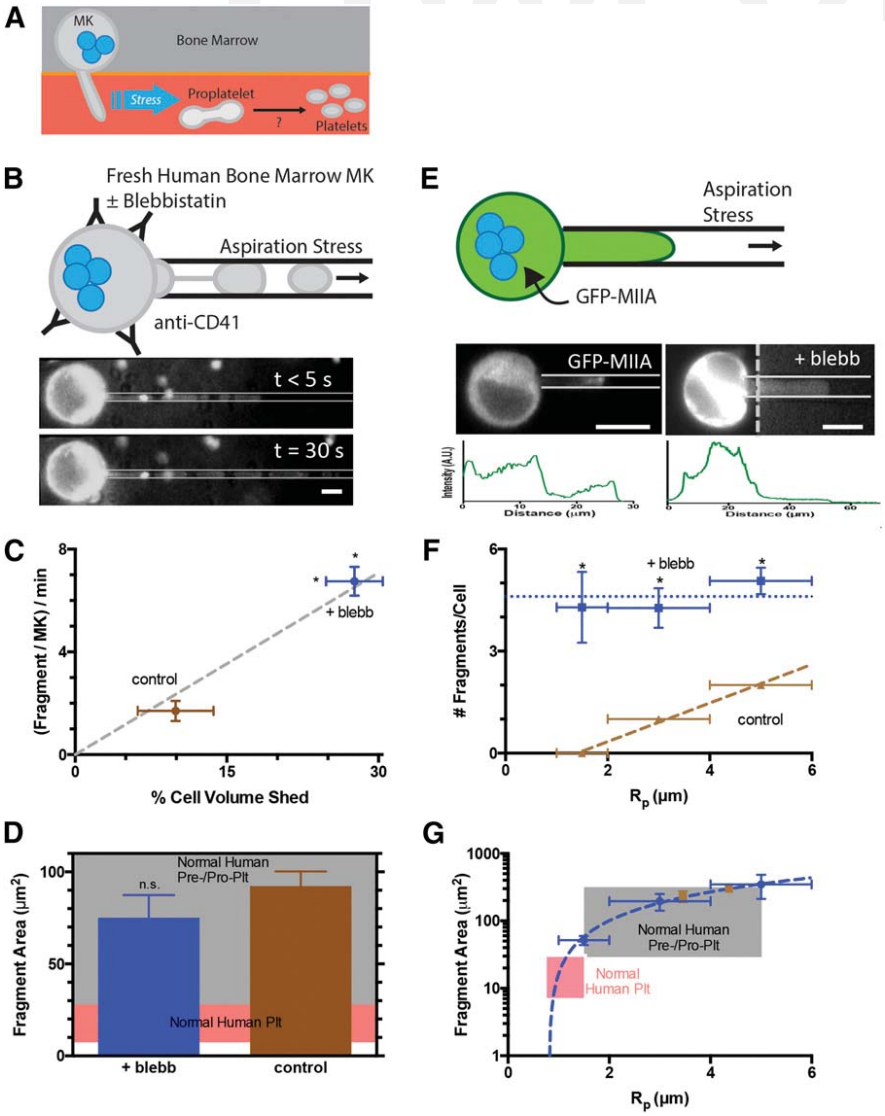

Figure 1. Myosin-IIA inhibition enhances fragments similar in size to normal human pre/proplatelets from in vitro micropipette aspiration. (A) Platelet generation scheme: MKs in bone marrow extend membrane processes into the flowing blood where shear stress fragments large pre/proplatelets. Conversion to dumbbell-shaped proplatelets allows fission to small, normal platelets. (B) MKs enriched from fresh human bone marrow aspirate stained with Hoechst 33342 and anti-CD41 were treated ± blebbistatin before micropipette aspiration. Fragmentation occurs within seconds and persists for minutes at physiologic stresses (scale bar = 10 μm). (C) Blebbistatin enhances fragment frequency and results in a higher percentage of total MK volume release vs DMSO control (N = 4 cells, n >10 fragments/cell for control, n >30 fragments/cell for blebb, ± SEM, $*P < .01$). The single-parameter fit goes through both data points. (D) Released fragment size is unaffected by blebbistatin, and fragments are similar in size to normal human pre/proplatelets (n = 35 fragments for control, n = 135 fragments for blebb, ±SEM, $P = .5$). The pink shaded region denotes the calculated range of area from normal human platelet diameters. The gray shaded region denotes estimations from reported preplatelet diameters.[2] (E) MEG-01 cells nucleofected with GFP-MIIA and treated ± blebbistatin and fluorescent images of GFP-MIIA MEG-01 cells undergoing fragmentation in micropipette aspiration (scale bar = 10 μm). Intensity of cell body has been adjusted to allow visualization of aspirated fragment. Intensity is plotted below each micrograph. (F) Blebbistatin treatment of non-nucleofected MEG-01 cells increases the number of fragments per cell as well as permission of fragmentation at smaller-radius pipettes. Linear fit of DMSO: $y = 0.57x - 0.8$, $R^2 = 0.99$, n = 2, ±SEM. 20 μM blebbistatin: n >15 ±SEM. Statistical significance determined between DMSO and 20 μM blebbistatin for a given R_p, $*P < .05$. (G) The fragment area is not affected by blebbistatin, but treatment facilitates fragmentation of smaller fragments from smaller pipettes. Linear fit of 20 μM blebbistatin: $y = 138x - 187$ ($R^2 = 0.99$, n <40, ±SEM). DMSO: n >6 ±SEM. The pink shaded region denotes calculated range of area from reported normal human platelet diameters. The gray shaded region denotes estimations from reported preplatelet diameters.[2]

Q:7

collected after their informed consent and institutional review board approval at the Children's Hospital of Philadelphia and the University of Pennsylvania. This study was conducted in accordance with the Declaration of Helsinki.

Rheometry and plateletlike particle generation

MEG-01 cells treated with dimethyl sulfoxide or 20 μM blebbistatin (72 hours) were washed, resuspended in Ca^{2+}-free Tyrode's + 1:1000 PGE1, and loaded onto a rheometer (Bohlin-Gemini). After 15 minutes of shear, samples were collected, labeled (supplemental Table 1), and analyzed by flow cytometry (LSR-II; BD Biosciences).

Functional characterization of MEG-01–derived PLPs

PLP activity was determined by collagen-I stimulation (100 μg/mL). Sheared samples as described before were labeled (supplemental Table 1) and analyzed by flow cytometry.

Micropipette aspiration

For fragmentation studies, MEG-01 cells were treated with ±20 μM blebbistatin for 72 hours and then washed and stained (supplemental Table 1). Studies of nucleofected MEG-01 cells were conducted within 48 hours of nucleofection. For cells treated with blebbistatin, cells were incubated at 37°C with 20 μM blebbistatin for 45 minutes, washed, and stained (supplemental Table 1). Capillary tubes of 1.0 mm I.D. (World Precision Instruments) were pulled into micropipettes using a Flaming-Brown Micropipette Puller (Sutter Instrument) and cut further using a de Fonbrune-type microforge (Vibratome) (< D > ~3 μm). A micropipette was attached to a dual-stage water manometer with reservoirs of adjustable height. Suction was applied by syringe, and the corresponding pressure was measured by a pressure transducer (Validyne) calibrated by a mercury U-tube manometer. Pressures for different experiments ranged from 0.5 to 20 kPa. Images were acquired using a Nikon Eclipse TE300 inverted microscope using a 40× objective and a Cascade CCD camera (Roper Scientific). Further image analysis was done using ImageJ software.

enrichment

Human peripheral blood was obtained by venipuncture and proplatelet fractions were enriched as previously described.[2,19] Samples were prepared for immunofluorescence or flow cytometry as described in the supplemental Methods and antibody incubation done (supplemental Table 1).

Results

Stress-induced fragments from MKs are large like pre/proplatelets and are maximized in number by inhibiting myosin-II

When primary human MKs from freshly isolated bone marrow are locally stressed by being pulled into small micropipettes with

diameters similar to human capillaries (~3 μm), aspiration facilitates the generation of $CD41^+$ fragments on ~minute-time scales (Figure1B and supplemental Figure 1). We have shown recently with MKs derived in culture from human bone marrow $CD34^+$ cells that such membrane projections in aspiration possess taxol-positive microtubules[5] similar to those seen in proplatelets and platelets.[20] Blebbistatin enhances fragmentation by ~fourfold (Figure 1C), and the simple geometry of each fragment within the micropipette compared with the quasispherical geometry of each MK reveals a linear relationship between fragment generation and volume shed by MKs. However, the projected area of these fragments proves to be independent of MII inhibition and fits within the broad range of pre/proplatelets (Figure 1D). Similar but more extensive results were obtained with the human megakaryocytic cell line, MEG-01, which has been used by others as a model for both human MK and platelet generation.[21,22] First, transfection of GFP-MIIA in these cells showed accumulation of MIIA over minutes toward the highly-stressed tip of the membrane projection (Figure 1E, left image), consistent with a mechanosensitive response of myosin-II in dictyostelium.[23] Blebbistatin treatment for 45 minutes before aspiration suppressed this stress-induced localization (Figure 1E, right image) and also enhanced fragmentation (Figure 1F). Although fragments per cell became independent of micropipette diameter with inhibition, fragment sizes decreased linearly with micropipette diameter independent of MII inhibition (Figure 1G and supplemental Figure 4A). The results thus indicate that downregulation of MII activity facilitates formation and fragmentation of MK projections, with $CD41^+$ fragment size consistently fitting within the broad range of pre/proplatelets.

Q:3

Optimal shear stress for PLP generation: maximal numbers with myosin-II inhibition

To assay for activity of $CD41^+$ fragments in sufficient bulk, a cone-and-plate rheometer was used to mimic in vitro the shear stress applied to MK projections in vivo (Figure 2A). Bone marrow–derived $CD34^+$ cells were cultured for 3 to 4 days in the presence of stem-cell factor and thrombopoeitin to direct differentiation toward MKs, and an additional 3 days of culture with blebbistatin to enhance polyploidy (supplemental Figure 1B) and MK maturation per our recent studies.[5] $CD41^+$ PLPs were also more abundant with MII inhibition, and shearing the treated MKs resulted in ~fivefold more PLPs relative to static untreated culture (Figure 2B). A shear stress of 2 Pascal (Pa) was used in accordance with arterial levels (1.5-3.0 Pa).[24] MEG-01 cells pretreated for 3 days with blebbistatin likewise showed greater polyploidy (supplemental Figure 1C) and produced two- to threefold more PLPs in static culture (Figure 2C). Combined with shear, MII inhibition resulted in up to fourfold more $CD41^+$ PLPs, with ~2 Pa emerging as an optimal shear stress, because higher shear stresses suppress fragmentation.

To assay PLP functionality, collagen-I–activated aggregation was measured by Annexin-V^+, 7-AAD^-, $CD41^+$ within the high-side-scatter population (Figure 2D) per earlier studies.[21] In the absence of collagen-I, aggregation was intrinsically low. Collagen-I stimulation of PLPs from $CD34^+$-derived MKs shows ~70% activation regardless of blebbistatin pretreatment, and this level of activation is independent of shear (Figure 2D, upper plot). MEG-01–derived PLPs show ~12% collagen-I–activated PLPs from static, untreated cultures and ~12% to 20% activated PLPs from blebbistatin-treated, sheared cultures (Figure 2D, lower plot). Although the MK-derived PLPs can be activated to a greater extent than MEG-01 PLPs, in the absence of collagen-I, baseline activation at the highest shear was two- to threefold higher compared with static or optimal shear. Such shear activation[25] might also underlie the decrease in PLP numbers at high shear (Figure 2C), which will be examined in a related context in the next section. Regardless, neither shear stress nor blebbistatin treatment affects this stimulated activation.

Scaling the absolute number of MEG-01–derived PLPs generated (Figure 2C) by the activation results (Figure 1D) provides a more accurate accounting of functional PLPs (Figure 2E). The optimum at 2 Pa shear emerges for 20 μM blebbistatin, with an ~eightfold increase in functional PLPs compared with those from static, untreated MEG-01 cultures. It is not known whether the optimum results from loss of functionality at high shear or high shear affecting fragmentation itself is addressed by investigating the MKs' response to shear stress.

Q:4

Myosin-IIA heavy chain is stress activated

Contractility of platelets is important for wound closure,[7] and we have recently found that primary hematopoietic stem cells maintain a high level of MIIA phosphorylated on S1943 (pS1943), which tends to deactivate MIIA (Figure 3A), and this phosphorylation generally decreases through differentiation.[5] Dephosphorylation is known to shift the equilibrium from soluble, cytoplasmic dimers toward assembled bipolar filaments[26] that interact with actin filaments in contributing to cell division, membrane rigidity, and strong adhesion to rigid matrices. MEG-01 cells (and $CD34^+$–derived MKs) show ~threefold higher pS1943 per MIIA than human platelets, suggesting higher basal tension in the platelets, and for both MEG-01 cells and fresh human platelets, 60 minutes of blebbistatin treatment increased the detectable pS1943 per MIIA by ~twofold (Figure 3B). Tail dephosphorylation thus transduces the mechanoenzymatic activity of the head (ie, MIIA is a mechanosensor).

If tension is exerted by the heads on the bipolar filament in the basal state, then applying further stress to cells could also increase filament tension as cells resist the stress, so that tail phosphorylation should decrease. Indeed, increasing shear stress on MEG-01 cells (Figure 2A) decreases MIIA pS1943 exponentially to ~threefold lower levels relative to static culture (Figure 3C), as confirmed by immunoblot (supplemental Figure 2A). The same kinetic expression also fits the decrease in PLP generation at shear stresses >2 Pa (Figure 2C). Importantly, 1-day-old human platelets exhibit the same low level of pS1943 as sheared MEG-01 (Figure 3C, star, and supplemental Figure 2B-D). Interstitial flows within the bone and marrow have been calculated to be nonzero,[27] but intravital imaging of MKs at their endothelial niche suggest much faster flow and higher shear within the vessel than within the interstitium.[1] Mature MKs in bone marrow are therefore likely shielded from fluid shear and should in principle maintain a high level of pS1943 to both enhance polyploidization (mimicked in vitro by blebbistatin) and suppress cortical rigidity during proplatelet extension and fragmentation (Figure 3C). Prolonged exposure to shear stress would then deplete pS1943 and thereby remove the block on MIIA activity to obtain a contractile phenotype *only* in circulating platelets. Our measurements on MEG-01 were done after 15 minutes of shear, consistent with intravital imaging,[1] which has suggested that MKs extend proplatelet pseudopods into blood in <15 minutes with fragmentation in ~30 minutes.

Visualization of GFP-MIIA with a phosphomimetic S1943D mutant of MIIA shows a uniform distribution along the aspirated length when stressed in micropipettes, and a nonphosphorylatable S1943A mutant shows a higher retention in the cell body and is depleted along the aspirated length (supplemental Figure 3A). Treating the cells with blebbistatin for 30 minutes before aspiration suppresses S1943A's decay along the aspirated projection,

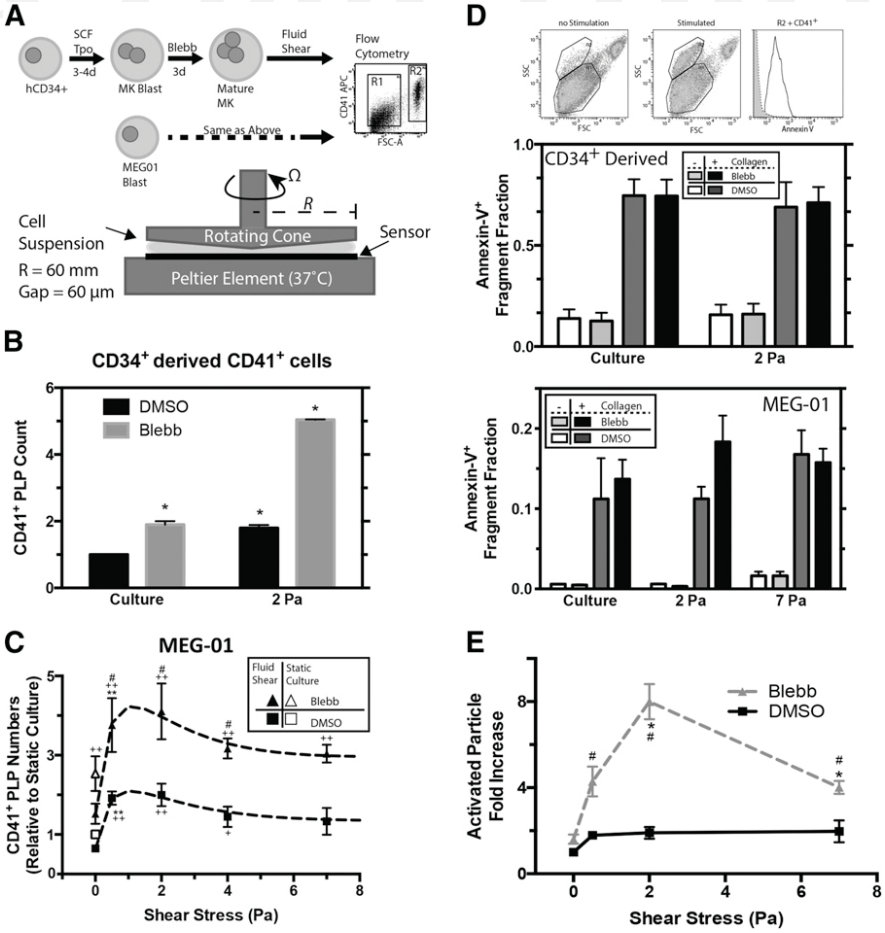

Figure 2. Shear stress and pharmacologic inhibition of myosin-II synergistically enhance PLP generation in vitro. (A) Myosin inhibition scheme and schematic of cone and plate rheometer. Primary human CD34$^+$ bone marrow–derived cells were cultured for 3 to 4 days in the presence of stem cell factor and thrombopoietin to drive differentiation toward MKs, followed by an additional 3 days of culture in the presence of 15 μM blebbistatin to promote polyploidy and MK maturation. In other experiments, MEG-01 cells were cultured for 3 days with 20 μM blebbistatin ($IC_{50} \approx 5$ μM). In either case, cell suspensions placed on the rheometer are subjected to controlled temperature (37°C for these studies), shear stress, stress duration, and gap size (60 μm for these studies). Samples collected from the rheometer are analyzed by flow cytometry to quantify PLP (R1) and nucleated cell (R2) fractions. (B) PLP quantitation after cone-and-plate rheometry of CD34$^+$-derived CD41$^+$ MKs shows an enhanced effect by both shear and MII inhibitions. Values are relative to unsheared, untreated cell culture (n = 3, ±SEM, * $P < .05$). (C) Quantitation of PLP generation after cone-and-plate imparted shear stress of MEG-01 cells (n = 6, ±SEM; *+#, $P < .05$; **++, $P < .005$; +, Significant from DMSO culture; #, significant from blebbistatin culture; *, significant from previous shear stress condition). The data are fit with a combination of a one-phase exponential decay and a one-site–specific binding model. DMSO fit: y = [2+4.0*exp(–0.62*x)]*[0.10+(0.66x/(0.65+x))], $R^2 = 0.97$). Bleb fit: y = [2+4.0*exp(–0.62*x)]*[0.26+(1.5x/(0.94+x))], $R^2 = 0.98$). (D) Activation of cone and plate generate PLP cell suspension from CD34$^+$-derived MKs (middle) or MEG-01 (lower). Sheared samples are stimulated by 100 μg/mL collagen-I and 1 mM $CaCl_2$, and activation is determined by a shift in side scatter and Annexin-V$^+$ CD41$^+$ 7AAD$^-$ (n = 3, ±SEM). (E) Considering the increased number of PLPs generated from MEG-01 shear (as in C), shear results in an ~8× net increase in functional PLPs compared with unsheared, untreated MEG-01 culture (n = 5, ±SEM, *+, $P < .05$; #, significant from untreated condition; *, significant from previous shear stress condition).

producing a more uniform S1943D phenotype for all (supplemental Figure 3B). Projections of aspirated membrane for the S1943D mutant and for blebbistatin-treated cells were also softer in distending more under high-aspiration stress than for wild-type (WT) or S1943A (supplemental Figure 3C). These results thus suggest that a high level of pS1943 favors proplatelet extension to facilitate fragmentation into the bloodstream (Figure 2B) while also ensuring that the resulting platelet population has relatively homogeneous MII levels among fragmented proplatelets. Such a posttranslational activation would be consistent with previous interpretations of the MIIA gene in mice, *Myh9*, as a negative regulator of platelet generation,[3] for which complete knockout causes defects in proplatelets and MK viability.[4]

Q:5

MYH9-RD mutants are not activated by stress

Mutations in the tail of MIIA can cause *MYH9*-RD, and each of the tail mutants D1424N, and E1841K studied here, are known to block myofilament assembly,[11] even when mixed with WT MIIA, which suggests dominant-negative phenotypes.[8] Patients expressing the E1841K mutation have macrothrombocytopenia with normal platelet aggregation but no change in platelet shape.[28] Here, peripheral blood samples from a patient with a D1424N mutation showed macrothrombocytopenia with increased platelet size and a reduced platelet count of 21.8 fL and 90 000/μL, respectively. Immunofluorescence imaging of MIIA and pS1943 in platelets that were allowed to spread on glass coverslips (Figure 4A) shows an absence of normal peripheral MIIA localization in patient platelets (Figure 4B). In contrast, pS1943 distribution remains diffuse in both normal and patient platelets, consistent with the imaging of the synthetic S1943D mutant. MIIA density is also decreased in patient platelets compared with normal (Figure 4C), which is consistent with previous studies of *MYH9*-RD showing up to a 50% deficiency in total MIIA[29]; in contrast, pS1943 densities are similar for normal and patient platelets (Figure 4D). A relative increase in phosphorylated

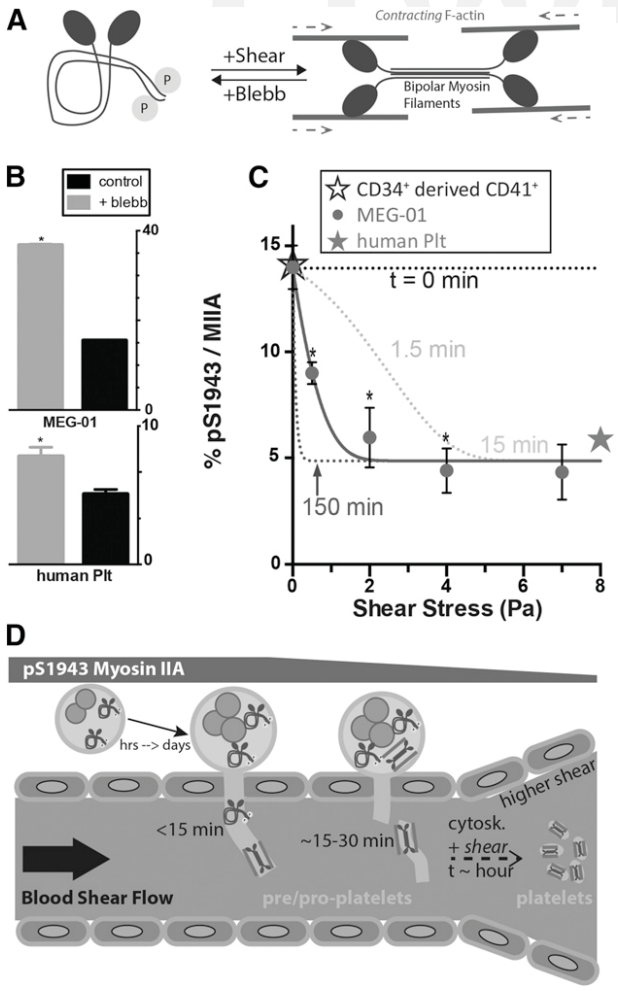

Figure 3. Stress activates myosin-II. (A) Schematic for how MIIA conformation and tail phosphorylation are stress-sensitive. (B) Blebbistatin decreases tension in MIIA filaments, and both MEG-01 cells analyzed by flow cytometry (upper) or platelets in fresh bone marrow aspirate (lower) show a similar increase in phosphorylation (n = 25 platelets, ±SEM, $*P < .001$). (C) MEG-01 cells sheared for 15 minutes show a shear dependent decay in S1943 phosphorylation (n = 4, ±SEM). %, the relative fluorescence intensity rather than stoichiometry. The stress- and time-dependent fit is: $\%pS1943/MIIA = A+B*\exp[(t/\tau)*(1-\exp(\sigma/\sigma_0)]$, where A = 4.9, B = 9.1, τ = 7.1 min, σ_0 = 1.6 Pa (R^2 = 0.98, $*P < .05$). Dashed lines are from this stress-dependent kinetic model. The solid star represents quantification of resting fresh human platelets and the open star represents the value of $CD34^+$-derived, $CD41^+$ mature MKs (n = 3 donors, ±SEM). (D) High ploidy, mature MKs localize to the perivascular niche, where they extend membrane extensions into the bloodstream within minutes that then fragment within 30 minutes by blood shear.[1] Although these initial fragments may be large and heterogeneous in size, additional exposure to shear can activate MIIA to facilitate cytofission to normal, small platelets. This process depends on MIIA activity and is sensitive to shear stress through loss of pS1943.

MIIA in patient platelets (Figure 4E) is consistent with suppressed contractility in patients and also with mechanosensing by normal MIIA (Figure 3B). The diffuseness of the patient's total MIIA is thus consistent with a significant fraction of MIIA being inactive.

Mean projected areas of platelets are larger for the patient as expected, with an increase from 6.9 μm^2 for normal to 19 μm^2 for D1424N patient platelets (Figure 4F). Because only 16% of patient platelets are within the size range of normal platelets (84% are much larger like pre/proplatelets), and because normal mouse proplatelets (with active MIIA) fragment in vivo over many hours after infusion,[19] direct mechanical fragmentation of proplatelets to platelets in vivo seems to have only a minor role in the absence of functional MIIA.

Platelet perimeters and calculated circularity[19] for normal platelets show a mixture of high circularity, small-perimeter normal platelets with dumbbell-shaped, large-perimeter proplatelets and high circularity, large-perimeter preplatelets (Figure 4G). Platelets from the *MYH9*-RD patient were predominately high circularity and large perimeter, corresponding to preplatelets (Figure 4G), consistent with previously noted effects of ethylenediaminetetraacetic acid (EDTA) anticoagulant repressing dumbbell-shaped proplatelets.[2] Past observations of a cleavage furrow[30] and a "snapping" back of the membrane after proplatelet fission[19] thus suggest a role for *active* myosin-II similar to that in cytokinesis of MK progenitors.[5]

A plot of normal peripheral thrombocrit levels from platelet count and size data of Thompson et al[31] shows that our D1424N patient has a peripheral thrombocrit level in the normal range (Figure 4H). Mouse models with the D1424N mutation have approximately twofold more MKs in the marrow than normal mice,[18] and if such compensation also occurred in humans, the patient thrombocrit level per MK approaches a linear fit of the normal data. These findings support a hypothesis for *MYH9*-RD defects in terminal platelet processing (Figure 4I), consistent with normal biogenesis of platelets in which pS1943 deactivates MIIA in earlier steps (Figure 2B). Thus in normal platelet generation, large pre/proplatelets sheared from the pS1943-rich processes that are extended by MKs can reversibly convert between proplatelets and preplatelets, but the pinching and subsequent fission to properly sized platelets is driven by MIIA. The conclusion that pre/proplatelets in *MYH9*-RD patients can be readily generated but cannot undergo fission helps to explain the increased MPV and decreased platelet count with reasonable maintenance of peripheral thrombocrit. Two key aspects of this model are examined next: (1) *MYH9*-RD mutants act as dominant negatives in stress-induced membrane fragmentation, and (2) normal MII activity is ultimately needed for cytofission to platelets.

MYH9-RD mutants exert dominant-negative effect in fragmentation of projections

Transient transfections of *MYH9*-RD mutants as GFP fusions in standard cell lines can help clarify mechanisms while minimizing variability and compensatory mechanisms. Indeed, the D1424N mutant in MEG-01 cells shows higher pS1943 per MIIA than cells overexpressing WT GFP-MIIA (Figure 5A), consistent with platelet findings (Figure 4E). In micropipette aspiration of MEG-01 cells expressing *MYH9*-RD mutants, the fluorescence along the aspirated projection appeared nearly flat and time-independent, as did blebbistatin-treated cells expressing the WT GFP-MIIA (Figure 5B-C). Fragments generated per cell were likewise similar for *MYH9*-RD mutants and for blebbistatin-treated MEG-01s (non-transfected), and all were significantly higher than DMSO-treated control, whereas they were zero for WT GFP-MIIA–overexpressing cells (Figure 5D). The transfected cell results thus suggest a dominant-negative effect of *MYH9*-RD on fragmentation because the constructs are overexpressed to mimic the stoichiometry of a heterozygous state, with immunostaining of total MIIA being ~60% higher in GFP-expressing cells than GFP-nonexpressing cells (supplemental Figure 5B-C). Consistent with past reports for granulocytes[16,17,29] and in contrast to WT GFP-MIIA that appeared cortical (supplemental Figure 5A), the *MYH9*-RD mutants expressed in MEG-01 cells suggested more GFP aggregates against a diffuse GFP signal—which we quantified in well-spread cells (supplemental Figure 5A). In addition, in micropipette aspiration of MEG-01s, the mutants did not affect fragment size (supplemental Figure 4), consistent with the aforementioned lack of size difference between fragments from blebbistatin-treated and control cells (Figure 1D).

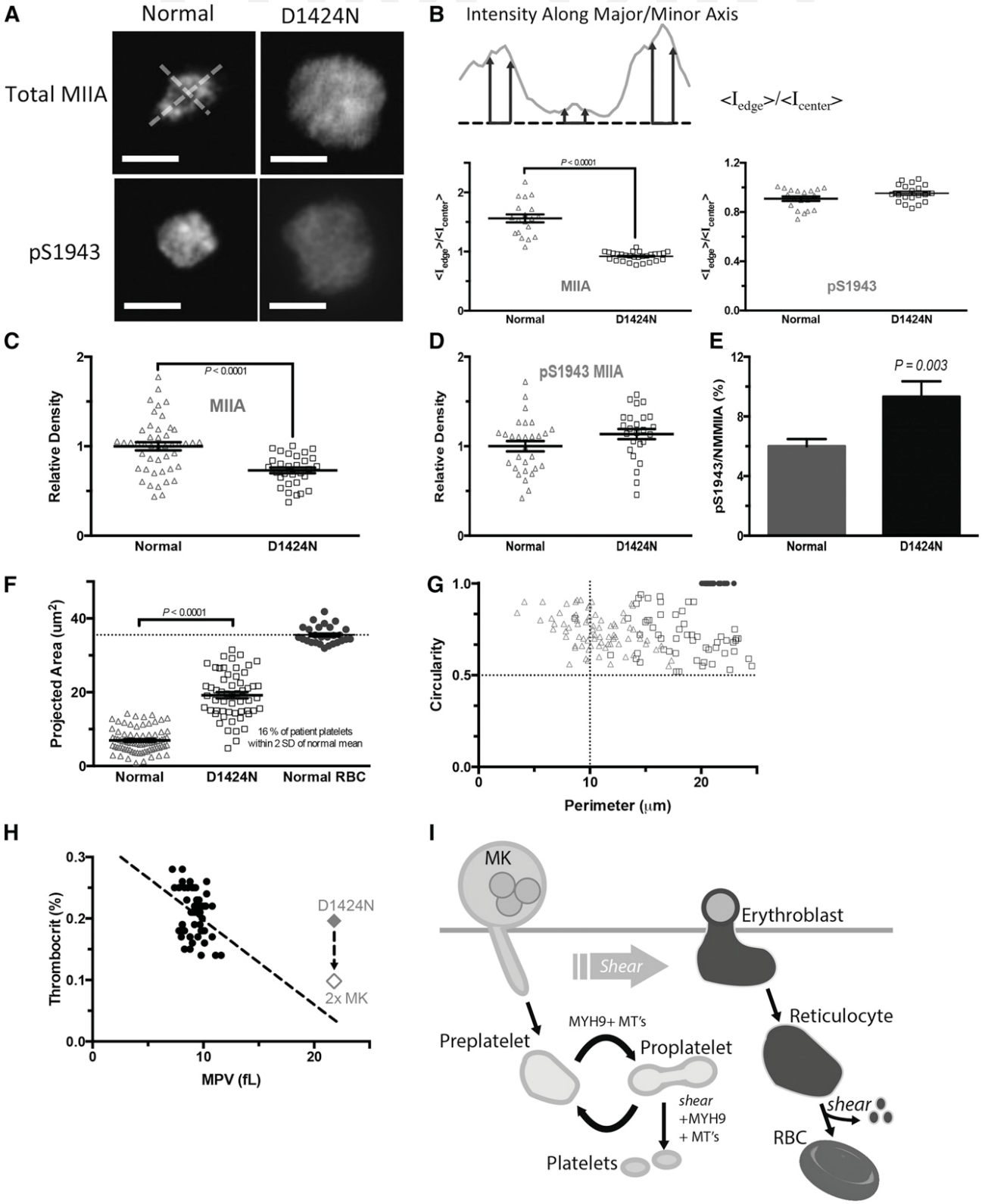

Figure 4. Characterization of abnormalities in *MYH9*-RD patient platelets. (A) Peripheral blood from a patient expressing c.4270G>A (D1424N) *MYH9*-RD mutation was collected in EDTA. Buffy coat was incubated with CD41-APC, anti-MIIA or anti-pS1943, and Hoechst 33342. Platelets were identified as $CD41^+$ $Hoechst^-$ (scale bar = 5 μm). (B) Peripheral MIIA is disrupted in platelets with the *MYH9*-RD mutation. Intensity line scans were made along perpendicular major and minor axes as shown. MIIA distribution is quantified by the ratio of average peripheral intensity to average center intensity. Total MIIA is peripheral in normal platelets and diffuse in mutant platelets, and phospho-MIIA is diffuse in either case. *MYH9*-RD mutation results in a decrease in total MIIA (C) but not in pS1943 MIIA expression (D). (E) Accounting for the maintenance of pS1943 density, but reduction in total MIIA, the patient platelets show an ~twofold increase in percent of phosphorylated MIIA. (F) Patient platelets show an increase in projected area. (G) *MYH9*-RD mutation has a dramatic effect on observed platelet shape (Normal: n = 83; D1424: n = 78; RBC: n = 32). Normal RBCs were used as a calibration control for (E-F). RBCs, red blood cells. (H) Thrombocrit values calculated from mean platelet volume (MPV), and platelet count data show a weak dependence on MPV (linear regression: thrombocrit = −0.01 * MPV + 0.33, $R^2 = 0.12$, n = 49).[31] The red diamond is the value for the D1424N patient. If a compensatory mechanism of increased MK

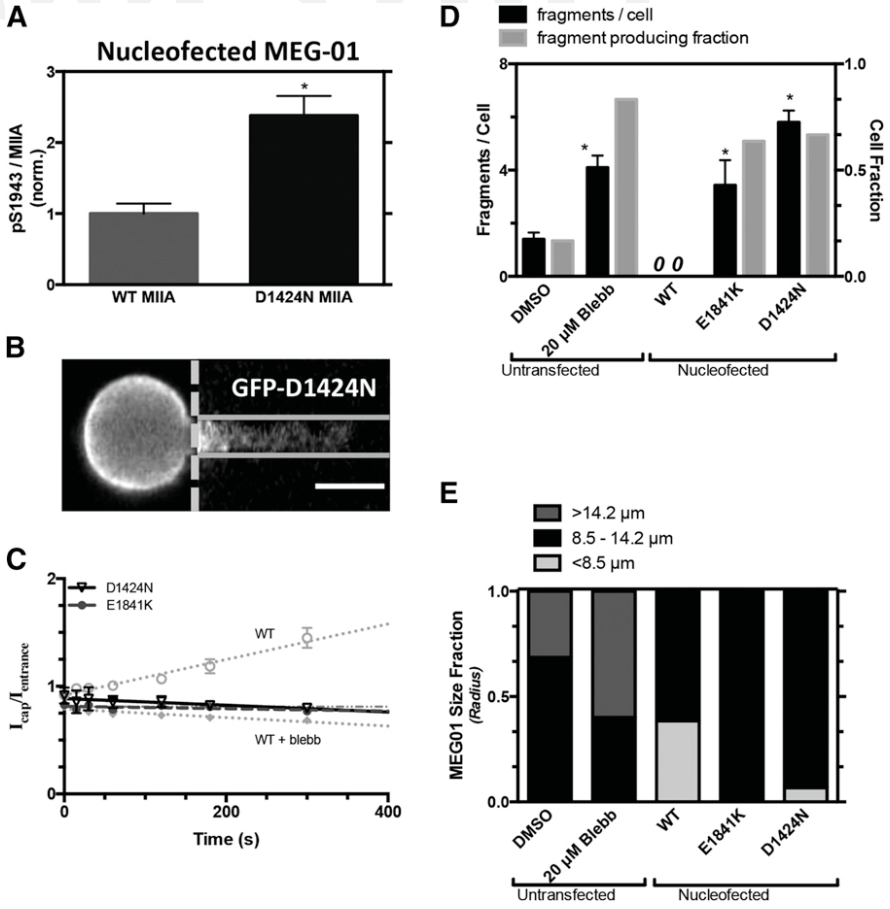

Figure 5. Stress-induced myosin-II localization and MK fragmentation altered by *MYH9*-RD. GFP-MIIA mutation associated with *MYH9*-RD, D1424N, or E1841K, specifically, were introduced into MEG-01 cells. (A) Introduction of a D1424N MIIA mutation in MEG-01 cells shows an increase in % pS1943 MIIA compared with WT by flow cytometry (*$P < .005$). (B) Representative fluorescent micrographs showing uniform GFP distribution from GFP-D1424N MIIA in MEG-01 (scale bar = 5 μm). (C) Upon application of stress by micropipette aspiration, GFP-MIIA is seen evenly distributed throughout the aspirated length in a manner similar to either S1943D MIIA or blebbistatin-treated cells (gray dotted line). E1841K: ($y = 1.1*10^{-4}x + 0.81$, $R^2 = 0.27$, n = 10, ±SEM). (D) These cells showed an enhanced propensity to produce fragments similar to that of blebbistatin treatment (n >8, ±SEM, *$P < .05$, significant from untransfected DMSO). (E) Quantification of MEG-01 size for each of the cell types used for micropipette aspiration. The *MYH9*-RD mutant cells, which produced fragments, show a higher distribution of larger cells compared with the WT and phosphomutants that did not fragment.

Cells overexpressing *MYH9*-RD mutants were slightly larger than cells overexpressing WT MIIA, despite similar GFP intensities (Figure 5E); however, DMSO control–treated MEG-01s were larger than transfected cells, whereas blebbistatin-treated cells were the largest (Figure 5E), consistent with their higher ploidy (supplemental Figure 1B-C). Because MK size relates to maturity[32] (ploidy, proplatelet extension, and platelet release), overexpression of normal MIIA tends to suppress size/maturity, whereas *MYH9*-RD mutants slightly increase MK size/maturity and disproportionately increase fragmentability (vs DMSO; Figure 5B). The possibility of a dominant-negative phenotype was tested with the D1424N mutant, which was cotransfected with mCherry-(WT MIIA): the GFP mutant colocalized strongly in aggregates with mCherry-(WT MIIA), whereas GFP-(WT MIIA) did not (supplemental Figure 5F).

Myosin-IIA activity is critical to pre/proplatelet fission to platelets

To determine whether normal MIIA activity is necessary for final fission to platelets, which seems defective in *MYH9*-RD, peripheral blood from healthy anonymous donors was enriched for proplatelets, as described by others.[2] Cultures at 37°C were treated for 1 or 6 hours with blebbistatin or nocodazole to, respectively, inhibit MII or depolymerize microtubules. Immunostaining for MIIA reveals that the normal peripheral distribution is made diffuse by blebbistatin but not by nocodazole (Figure 6A-B). In addition, MIIA localizes to the cleavage furrow of proplatelets, and immunostaining for the other hematopoietic isoform,[9] MIIB, indicated a relative intensity of MIIA:MIIB ~250, that confirms MIIA as the relevant isoform. Quantitation of circularity and perimeter per recent studies[2] suggests that small perimeter platelet populations always dominate, but both drug treatments enrich for the large discoidal preplatelet populations compared with DMSO controls (Figure 6C). Relative to the barbell-shaped proplatelets, the preplatelets shift from ~1:3 for DMSO control cultures to ~40:1 for blebbistatin treatment and ~8:1 for nocodazole treatment (Figure 6C). No significant difference between 1 and 6 hours suggests that the transition takes tens of minutes or less, which is consistent with the mechanoactivation kinetics of MIIA (supplemental Figure 3) and also with cytokinesis in mitosis.[5] Although both MIIA and microtubule activity drive these conversions, inhibition of MIIA alone generates large platelets with diffuse MIIA that appear similar to *MYH9*-RD platelets (compare Figure 6A-B with Figure 4A).

Flow cytometry was done on whole-blood samples after treating for 1 hour with DMSO, blebbistatin, or nocodazole. Populations were

Figure 4 (continued) number applies as described for mouse,[18] the *MYH9*-RD patients' thrombocrit values also fit the trend of normal thrombocrit values. (I) Proposed model of platelet generation accounting for *MYH9*-RD induced macrothrombocytopenia, with MK shedding of preplatelets being analogous to erythroblast enucleation, where the circulating reticulocyte becomes a discocyte through the aid of hydrodynamic shear force. MIIA evidently has no role because RBCs appear normal in *MYH9*-RD blood. Blood shear forces likewise assist the transition from preplatelet to proplatelet, but MIIA drives cleavage furrow formation and fission, resulting in small normal platelets. *MYH9*-RD mutations abrogate normal MIIA activity, preventing cleavage furrow formation and platelet fission, thus causing an increase in circulating preplatelets and the phenotypic large platelets.

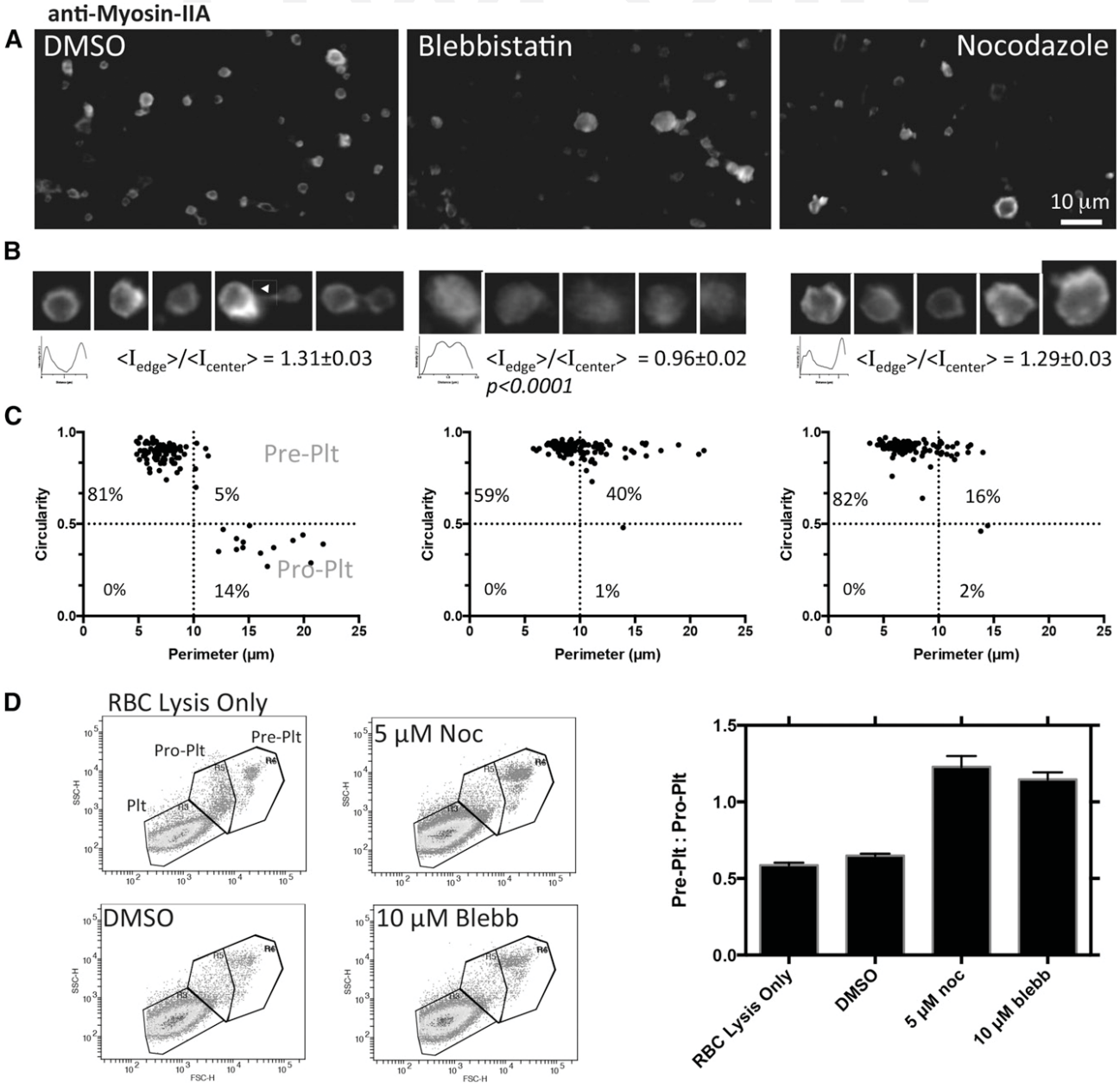

Figure 6. Myosin-IIA activity controls conversion to proplatelets and cleavage of normal platelets. Proplatelet-enriched fractions from peripheral blood collected in AJ buffer were incubated with DMSO, 10 μM blebbistatin, or 5 μM nocodazole for 6 hours at 37°C. (A-B) Imaging after drug treatment shows at high magnification of the myosin IIA distribution as well as its morphology. Line scans and surface plots show that myosin localization to the periphery with DMSO and nocodazole treatment is disrupted by blebbistatin. Staining for MIIB was done in parallel using the same secondary antibody, which indicated, on average, MIIA:MIIB = 250 (N = 25 across 5 fields of view for each isoform). (C) Quantification of immunofluorescence of 6-hour–treated proplatelet-enriched fractions shows a shift toward preplatelets at the expense of proplatelets after blebbistatin or nocodazole incubation. One-hour treatments done in parallel did not show a significant difference from 6-hour treatments. Gates are based on previously published values.[2] (D) Flow cytometry scatter plots with platelet populations determined based on scatter and gated on $CD41^+$ $Hoechst^-$ GPA^-. The bar graph summarizes flow cytometry.

determined from scatter of normal human platelets and calibration beads, and events of interest were gated as $CD41^+$, $Hoechst^-$, GPA^-. In agreement with immunofluorescence, drug treatment compared with control showed a significant increase in the ratio of preplatelets to proplatelets, resulting from an increase in preplatelets at the expense of proplatelets (Figure 6D).

Discussion

This is the first study to demonstrate a regulated synergy between MIIA activity and applied stress, with shear stress enhancing MIIA activity by reducing phospho-S1943 to promote myofilament assembly. The findings resolve an apparent paradox in MK/platelet poiesis that arose with past findings that drug inhibition of myosin-II is useful, whereas *MYH9* mutants exhibit defects. Normal MKs indeed suppress MIIA activity to increase ploidy and to be pliable enough for fragmentation under shear (Figure 1A). *MYH9*-RD mutations (at least in MIIA's tail) likewise favor fragmentation, but shear reactivation of MIIA that normally occurs in human platelets to drive cytofission is lacking in *MYH9*-RD pre/proplatelets, which remain large (Figure 4E). Stress is thus an external cue to activate MIIA locally (Fig.S3). Drug inhibition of MIIA also softens the membrane to favor fragmentation to sizes similar to normal human pre/proplatelets

(Figure 1D). Although microtubules also affect pre/proplatelets,[2] tubulin levels are unaffected in mutants here,[29] so that the macrothrombocytopenia is caused by an MIIA-limiting cytofission failure and not by a thrombocrit defect (Figure 4H). Lineage-specific *Myh9* knockout mice likewise show more and larger MKs that clearly extend pre/proplatelets,[14] and both D1424N and E1841K transgenic mice exhibit macrothrombocytopenia with slightly higher thrombocrit levels.[18] Switchable activity of MIIA is therefore crucial to the biogenesis of normal small platelets, which require active MIIA to contract wounds.

MYH9 expression appears downstream of p53, which is normally repressed to permit the high ploidy of MKs.[33] Knockdown of p53 indeed downregulates *MYH9*, *ACTA2*, and *FLNA*, all of which contribute to actomyosin forces, and so p53 defects may also cause platelet size abnormalities. MII activity in early MKs with and without *MYH9*-RD mutation could also be very different, as suggested by MK adhesion forces,[34] and also from the fact that MIIB is normally high in early MKs but dysregulated in some diseases.[9,35] Myosin-II isoforms thus receive cues from the microenvironment to choreograph key spatio-temporal mechanisms of cell growth, differentiation, and changes in cell shape.

Acknowledgments

This study was supported by the National Institutes of Health (R01-EB007049, R01-HL062352, P01-DK032094, NCATS-8UL1TR000003, P30-DK090969) and the National Science Foundation's Materials Research Science and Engineering Center.

Authorship

Contribution: K.R.S. and J.-W.S. performed experiments; K.R.S. analyzed results; K.R.S. and D.E.D. designed research and wrote the paper; and M.P.L. provided *MYH9*-RD patient samples and contributed council.

Conflict-of-interest disclosure: The authors declare no competing financial interests.

Correspondence: Dennis E. Discher, University of Pennsylvania, 129 Towne Building, Philadelphia, PA 19104; e-mail: discher@seas.upenn.edu. Q:6

References

1. Junt T, Schulze H, Chen Z, et al. Dynamic visualization of thrombopoiesis within bone marrow. *Science.* 2007;317(5845):1767-1770.
2. Thon JN, Macleod H, Begonja AJ, et al. Microtubule and cortical forces determine platelet size during vascular platelet production. *Nat Commun.* 2012;3(May):852.
3. Chen Z, Naveiras O, Balduini A, et al. The May-Hegglin anomaly gene MYH9 is a negative regulator of platelet biogenesis modulated by the Rho-ROCK pathway. *Blood.* 2007;110(1):171-179.
4. Eckly A, Rinckel J-Y, Laeuffer P, et al. Proplatelet formation deficit and megakaryocyte death contribute to thrombocytopenia in Myh9 knockout mice. *J Thromb Haemost.* 2010;8(10):2243-2251.
5. Shin J-W, Swift J, Spinler KR, Discher DE. Myosin-II inhibition and soft 2D matrix maximize multinucleation and cellular projections typical of platelet-producing megakaryocytes. *Proc Natl Acad Sci USA.* 2011;108(28):11458-11463.
6. Maupin P, Phillips CL, Adelstein RS, Pollard TD. Differential localization of myosin-II isozymes in human cultured cells and blood cells. *J Cell Sci.* 1994;107(Pt 1):3077-3090.
7. Lam WA, Chaudhuri O, Crow A, et al. Mechanics and contraction dynamics of single platelets and implications for clot stiffening. *Nat Mater.* 2011; 10(1):61-66.
8. Franke JD, Dong F, Rickoll WL, Kelley MJ, Kiehart DP. Rod mutations associated with MYH9-related disorders disrupt nonmuscle myosin-IIA assembly. *Blood.* 2005;105(1):161-169.
9. Shin J-W, Buxboim A, Spinler KR, et al. Contractile forces sustain and polarize hematopoiesis from stem and progenitor cells. *Cell Stem Cell.* 2014;14(1):81-93.
10. Seri M, Pecci A, Di Bari F, et al. MYH9-related disease: May-Hegglin anomaly, Sebastian syndrome, Fechtner syndrome, and Epstein syndrome are not distinct entities but represent a variable expression of a single illness. *Medicine (Baltimore).* 2003;82(3):203-215.
11. Balduini CL, Pecci A, Savoia A. Recent advances in the understanding and management of MYH9-related inherited thrombocytopenias. *Br J Haematol.* 2011;154(2):161-174.
12. Kelley MJ, Jawien W, Ortel TL, Korczak JF. Mutation of MYH9, encoding non-muscle myosin heavy chain A, in May-Hegglin anomaly. *Nat Genet.* 2000;26(1):106-108.
13. Godwin HA, Ginsburg AD. May-Hegglin anomaly: a defect in megakaryocyte fragmentation? *Br J Haematol.* 1974;26(1):117-128.
14. Eckly A, Strassel C, Freund M, et al. Abnormal megakaryocyte morphology and proplatelet formation in mice with megakaryocyte-restricted MYH9 inactivation. *Blood.* 2009;113(14):3182-3189.
15. Seri M, Cusano R, Gangarossa S, et al; The May-Hegglin/Fechtner Syndrome Consortium. Mutations in MYH9 result in the May-Hegglin anomaly, and Fechtner and Sebastian syndromes. *Nat Genet.* 2000;26(1):103-105.
16. Pecci A, Canobbio I, Balduini A, et al. Pathogenetic mechanisms of hematological abnormalities of patients with MYH9 mutations. *Hum Mol Genet.* 2005;14(21):3169-3178.
17. Savoia A, De Rocco D, Panza E, et al. Heavy chain myosin 9-related disease (MYH9 -RD): neutrophil inclusions of myosin-9 as a pathognomonic sign of the disorder. *Thromb Haemost.* 2010;103(4):826-832.
18. Zhang Y, Conti MA, Malide D, et al. Mouse models of MYH9-related disease: mutations in nonmuscle myosin II-A. *Blood.* 2012;119(1):238-250.
19. Thon JN, Montalvo A, Patel-Hett S, et al. Cytoskeletal mechanics of proplatelet maturation and platelet release. *J Cell Biol.* 2010;191(4):861-874.
20. Italiano JE Jr, Lecine P, Shivdasani RA, Hartwig JH. Blood platelets are assembled principally at the ends of proplatelet processes produced by differentiated megakaryocytes. *J Cell Biol.* 1999; 147(6):1299-1312.
21. O'Brien JJ, Spinelli SL, Tober J, et al. 15-deoxy-delta12,14-PGJ2 enhances platelet production from megakaryocytes. *Blood.* 2008;112(10):4051-4060.
22. Takeuchi K, Satoh M, Kuno H, Yoshida T, Kondo H, Takeuchi M. Platelet-like particle formation in the human megakaryoblastic leukaemia cell lines, MEG-01 and MEG-01s. *Br J Haematol.* 1998; 100(2):436-444.
23. Ren Y, Effler JC, Norstrom M, et al. Mechanosensing through cooperative interactions between myosin II and the actin crosslinker cortexillin I. *Curr Biol.* 2009;19(17):1421-1428.
24. Schubert A, Cattaruzza M, Hecker M, Darmer D, Holtz J, Morawietz H. Shear stress-dependent regulation of the human beta-tubulin folding cofactor D gene. *Circ Res.* 2000;87(12):1188-1194.
25. Lu Q, Hofferbert BV, Koo G, Malinauskas RA. In vitro shear stress-induced platelet activation: sensitivity of human and bovine blood. *Artif Organs.* 2013;37(10):894-903.
26. Alberts B, Johnson A, Lewis J, et al. Molecular Biology of the Cell. New York: Garland Science; 2007.
27. Weinbaum S, Cowin SC, Zeng Y. A model for the excitation of osteocytes by mechanical loading-induced bone fluid shear stresses. *J Biomech.* 1994;27(3):339-360.
28. Canobbio I, Noris P, Pecci A, Balduini A, Balduini CL, Torti M. Altered cytoskeleton organization in platelets from patients with MYH9-related disease. *J Thromb Haemost.* 2005;3(5):1026-1035.
29. Deutsch S, Rideau A, Bochaton-Piallat M-L, et al. Asp1424Asn MYH9 mutation results in an unstable protein responsible for the phenotypes in May-Hegglin anomaly/Fechtner syndrome. *Blood.* 2003;102(2):529-534.
30. Schwertz H, Köster S, Kahr WH, et al. Anucleate platelets generate progeny. *Blood.* 2010;115(18): 3801-3809.
31. Thompson CB, Jakubowski JA. The pathophysiology and clinical relevance of platelet heterogeneity. *Blood.* 1988;72(1):1-8.
32. Mattia G, Vulcano F, Milazzo L, et al. Different ploidy levels of megakaryocytes generated from peripheral or cord blood CD34+ cells are correlated with different levels of platelet release. *Blood.* 2002;99(3):888-897.
33. Apostolidis PA, Lindsey S, Miller WM, Papoutsakis ET. Proposed megakaryocytic regulon of p53: the genes engaged to control cell cycle and apoptosis during megakaryocytic differentiation. *Physiol Genomics.* 2012;44(12):638-650.
34. Chen Y, Boukour S, Milloud R, et al. The abnormal proplatelet formation in MYH9-related macrothrombocytopenia results from an increased actomyosin contractility and is rescued by myosin IIA inhibition. *J Thromb Haemost.* 2013;11(12): 2163-2175.
35. Bluteau D, Glembotsky AC, Raimbault A, et al. Dysmegakaryopoiesis of FPD/AML pedigrees with constitutional RUNX1 mutations is linked to myosin II deregulated expression. *Blood.* 2012; 120(13):2708-2718.

Supplementary Materials and Methods

Materials For washing or antibody staining of cells, PBS without Ca^{2+} or Mg^{2+} (Invitrogen) was supplemented with 1% BSA (Sigma-Aldrich). For cell culture, RPMI-1640, penicillin-streptomycin, and FBS were all purchased from Invitrogen. For Western analysis, protease inhibitor mixture was purchased from Sigma. For flow cytometry, 7-Amino-actinomycin D (7-AAD) was purchased from Sigma and Hoeschst 33342 was purchased from Invitrogen. The (±)-blebbistatin was purchased from EMD Biosciences. Prostaglandin E1 was purchased from Sigma. Adenosine, theophylline, citrate, and Percoll was purchased from Sigma.

Antibodies Primary antibodies used for flow cytometry, Western blotting, and imaging include anti-human CD41-PE or –APC (eBioscience), anti-Annexin V-PE (BD Biosciences), non-muscle myosin-II (MIIA) (Sigma), phosphorylated S1943 MIIA (pS1943 MIIA) (Cell Signaling), β-actin (Santa Cruz). Secondary antibodies include donkey anti-rabbit Alexa 488 (Invitrogen), donkey anti-rabbit Alexa 647 (Invitrogen), and anti-mouse or anti-rabbit HRP-conjugated IgG (GE Healthcare).

Cell Culture and Transient Nucleofection MEG-01 cells were obtained from ATCC and maintained in RPMI-1640 supplemented with 10% FBS and 1% antibiotics. Cells were transfected using an Amaxa Nucleofector kit according to the manufacturer's instructions (Lonza). Briefly, 10^6 cells were resuspended in the nucleofector solution and supplement provided in the kit. DNA was added and the sample was placed in the Nucleofector Device. Cells were then incubated at room temperature for no more than five minutes followed by addition of 1 mL of pre-warmed RPMI-1640 medium and transfer to 6 well plates containing 1 mL of pre-warmed RPMI-1640 per well. Medium was exchanged two times 24 hours after nucleofection. Transfected cells were viable for 2-3 days as confirmed by exclusion of 7AAD staining. Transfection efficiency was ~5% to ~10% for GFP-tagged MIIA constructs (WT, S1943D, S1943A, D1424N, E1841K).

$CD34^+$ bone marrow derived cells were obtained from the University of Pennsylvania Stem Cell and Xenograft Core. Cells were cultured for 3-4 days in the presence of SCF and Tpo (R&D Systems) in Stem Span SFEM II (Stem Cell Technologies) supplemented with 1% antibiotics. After this brief cytokine culture, cells were used as described throughout for MEG-01.

***MYH9*-RD Transfection and Immunofluorescence** A549 cells were used as they are easily transfected and adherent, which simplifies imaging. Cells were seeded on 18 mm^2 circular microscope cover slips in a 6 well plate and allowed to adhere overnight in F-12 growth media (Life Technologies) supplemented with 10% FBS and 1% antibiotics. *MYH9* constructs were introduced via transfection using Lipofectamine 2000 (Life Technologies) as per the manufactures protocol. Briefly, media was removed from cells and replaced with 800 µL Opti-MEM (Life Technologies) per well. Two cocktails were prepared for each reaction. Cocktail A consisted of 7 µL Lipofectamine 2000 + 93 µL Opti-MEM. Cocktail B consisted of 3 µg DNA + Opti-MEM to bring total volume to 100 µL. A and B were combined and after 5 minutes were added dropwise to each well. Cells were incubated for ~5 hours at 37°, 5% CO_2 after which media was replaced with F-12 growth media and allowed to incubate overnight.

The following protocol was followed for visualizing *MYH9*-RD induced myosin aggregates as well as myosin expression in *MYH9*-RD patient platelets. Cells were briefly fixed with 4% paraformaldehyde followed by three PBS washes. Next, cells were permeabilized with 0.5% Triton X-100 then blocked using 3% BSA + 0.05%

Tween-20. Either total myosin or pS1943 myosin primary antibody was added at 1:100 by dilution with blocking buffer and incubated for 5-6 hours at room temperature. Cells were washed three times with PBS and either Alexa 488 or Alexa 647 secondary antibody was added at 1:400 diluted with PBS. For patient platelet experiments, CD47-APC was added at 1:100. After incubation at room temperature for 60 minutes, cells were washed twice followed by addition of Hoescht 33342 1:10,000, incubation at room temperature for 5 minutes, and another two PBS washes. Cover slips were then mounted on slides using ProLong Gold Antifade Reagent (Life Technologies), sealed with nail polish, and cured for 24 hours before imaging. Images were acquired using an Olympus IX71 inverted microscope with a 300W Xenon lamp illumination using 40x, 60x, or 150x objectives with or without 1.6x multiplication. Further image analysis was done using ImageJ (National Institutes of Health).

Proplatelet Fraction Enrichment, Treatment, Imaging, and Flow Cytometry Human peripheral blood was obtained by venipuncture and collected into 10% (v/v) AJ buffer (85mM sodium citrate, 69mM citric acid, 20mg/ml glucose). Proplatelet fractions were enriched and treated as previously described (e.g. Thon, *et al, JCB* 2010 and Thon, *et al, Nat Commun* 2012). Briefly, peripheral blood samples were centrifuged for 20 minutes at 180g. Buffy and PRP was transferred to a new tube and spun for 15 minutes at 180g. Buffy and PRP was transferred to a new tube and spun for 15 minutes at 1000g. The pellet was resuspended in Tyrode's Buffer and treated for 1-6 hours with DMSO, 10μM blebbistatin, or 5μM nocodazole at 37°C. After treatment, samples were seeded onto poly-L-lysine (1μg/ml) coated coverslips, allowed to adhere for 15min at RT, and fixed with 4% paraformaldehyde. Samples were prepared for immunofluorescence as described above and antibody incubation done per Table S1.

Proplatelet Flow Cytometry Human peripheral blood collected as described above was immediately fixed with 4% paraformaldehyde and RBCs lysed with 2 volume equivalents RBC Lysis Buffer (Sigma) for 10 minutes at 37°C. For drug treatment, whole blood was treated with DMSO, 10μM blebbistatin, or 5μM nocodazole at 37°C before fixation/lysis. Fixed and lysed samples were washed twice, resuspended in Tyrode's buffer and antibody incubation done per Table S1 and run on a BD LSRII.

Enrichment of Human Bone Marrow Whole human bone marrow aspirate was obtained from the University of Pennsylvania Stem Cell and Xenograft Core. Enrichment of megakaryocytes and platelets was adapted from previously published methods (e.g. Ishibashi, *et al*, *Blood* 1986). Briefly, aspirate was pipetted repeatedly to generate a single cell suspension. Whole marrow was mixed with an equal volume of CATCH buffer (2% BSA, 1 mM adenosine, 2 mM theophylline, 13.6 mM citrate, 11.1 mM glucose, pH 7.0, 290 mOsm in PBS). 1.02 g/mL and 1.05 g/mL Percoll solution was made by addition of 1.5 M NaCl to Percoll stock. 4 mL of CATCH/Marrow was added to 3 mL of 1.02 g/mL Percoll, gently layered over 4 mL of 1.05 g/mL Percoll, and spun at 400g for 20 minutes. The MK enriched interface and ~2 mL of the upper phase was collected and washed by addition of 2 volume equivalents CATCH and spun at 300g for 10 minutes. Supernatant was removed and pellet was washed again with CATCH. Washed cells were treated ± blebbistatin and used for micropipette aspiration and immunofluorescence as described above.

Western Blotting In general, cells were washed with ice-cold PBS and lysed on ice with lysis buffer (150 mM sodium chloride, 1% Nonidet P-40, 1% protease inhibitor mixture, 1 mM activated sodium orthovanadate, 50 mM Tris at pH 8.0) for 30 minutes. Whole lysates were separated on 3%-8% SDS/PAGE gels (NuPAGE 3-8% Tris-Acetate, Invitrogen). The proteins were then transferred to a polyvinylidene fluoride (PVDF) membrane with an iBlot Gel Transfer Device (Invitrogen), followed by blocking with 5% nonfat dry milk solution for 1 hour. Incubation with primary antibodies was done at 4°C overnight with 1:1000 β-actin or 1:1000 HSP90, and 1:1000 MIIA or pS1943 MIIA antibodies. After washing, the membrane was incubated with 1:2500 anti-rabbit and 1:2500 anti-mouse HRP-conjugated IgG antibodies at room temperature for 1 hour. The blot was developed with ChromoSensor (GenScript) for 5 minutes, followed by digital scanning to perform densitometry analysis by ImageJ.

Statistical Analysis All statistical analyses were performed using GraphPad Prism 4. Unless otherwise noted, all statistical comparisons were made by unpaired two-tailed Student *t* test and were considered significant if $P < 0.05$.

Supplementary Figure Legends

Table S1. List of antibodies described in Methods. Detailed antibody incubation protocol for specific experiments.

Figure S1. Pharmacological inhibition of megakaryocyte myosin. (A) Micrographs of micropipette aspiration of MK enriched human bone marrow aspirate. Nucleated white blood cells (*upper,* red circles) are Hoescht^{+} but CD41^{-} (*bottom*), the MK being micropipette aspirated is Hoescht^{+} and CD41^{+}, and surrounding platelets are Hoescht^{-} and CD41^{+}. (B) Myosin II inhibition by 72 hour blebbistatin culture increases ploidy of CD34^{+} derived CD41^{+} cells (n=4, *P<0.01). (C) MEG-01 cells treated with DMSO, 20 μM, or 50 μM blebbistatin for 72 hrs likewise show ~3 fold increase in 4n cells and >20 fold increase in higher ploidy (≥8n) cells (n=15, *P<0.005).

Figure S2. Phosphorylation of resting fresh human platelets. (A) The immunoblots confirm specificity of the antibodies used in immunofluorescence in Figs. 3,4,5,6, and they also confirm the shear dependent decrease in pS1943 per MIIA shown at the single cell level for MEG-01 cells in Fig.3C. Raw scans of the same blot are presented without manipulation. Blots were probed with indicated antibodies, developed, and scanned (**left**). Blots were then stripped and re-probed with different antibodies, developed, and scanned (**right**). Absence of HSP90 band in lower right scan confirms efficiency of stripping. In lower blots, 1x cell loading =

$4x10^6$ MEG-01 cells. (B) Fresh human platelets were analyzed with flow cytometry and gated on CD41 for either total MIIA (*left*), or pS1943 MIIA (*middle*). The histogram illustrates the resultant distribution of total MIIA or pS1943 MIIA and the mean of each distribution is captured by the vertical lines (B, *right*). (C) Individual events were analyzed. Bins were created to include equal number of events per bin. The linear fit of total MIIA: $y=2.4x+19$, $R^2=0.99$. Linear fit of pS1943 MIIA: $y=0.2x-0.9$, $R^2=0.99$. (D) The ratio of pS1943 to total MIIA was calculated by dividing the linear fits from panel B. The fit: $y=[0.1x/(8+x)]-0.05$, $R^2=0.99$, $<pS1943/MIIA> = 0.06$.

Figure S3. MIIA activity impacts localization and MEG-01 membrane stiffness. (A) Representative fluorescent micrographs of nucleofected MEG-01 cells during micropipette aspiration. All scale bars = 10 μm. GFP-WT MIIA shows accumulation at the tip, GFP-S1943D MIIA shows uniform distribution along the aspirated length, GFP-S1943A MIIA shows depletion at the tip. (B) Treatment with blebbistatin recovers a uniform distribution regardless of construct ($n>10$, ±SEM, $*P<0.05$, statistical significance determined between ±blebbistatin for a given construct at a given time point). (C) MEG-01 membrane stiffness is affected by introduction of GFP tagged MIIA constructs by nucleofection. Cells phosphomimetic introduced with the phosphomimetic S1943D mutant show a similar membrane softening as is seen by pharmacological treatment of untransfected cells with blebbistatin (D) ($N>25$ cells, ±SEM).

Figure S4. Effect of *MYH9*-RD on fragmentation size. (A) Fragment volume is not affected by blebbistatin; however, blebbistatin treatment facilitates fragmentation of smaller fragments from smaller radius pipettes. Pink shaded region denotes calculated range of volume from reported normal human platelet diameters. Gray shaded region denotes calculated range of volume from reported preplatelet diameters.[2] Both shaded regions calculated using reported diameters and assuming ellipsoid shape. Linear fit of 20 μM Blebbistatin: $y=84x-68$ ($R^2=0.9956$, $n<40$, ±SEM). DMSO: $n>6$, ±SEM. (B) Fragmentation of MEG-01 cells following introduction of E1841K GFP-MIIA. *MYH9*-RD mutation does not significantly impact either fragment area (B) nor fragment volume (C) compared to DMSO treated MEG-01 (dashed line) ($N\geq10$, ±SEM).

Figure S5. Quantification and visualization of MIIA overexpression. (A) Lipofection was used to introduce GFP-MIIA constructs in A549 cells. These cells were used for imaging instead of spherical MEG-01 because the highly adherent A549 cells are generally well-spread and thus easier to focus on all aggregates for quantitation. Immunofluorescence reveals abnormal myosin aggregates that are enriched in GFP-MIIA compared to surrounding cytoplasm (scale bar = 10 μm). (B) Total MIIA overexpression in GFP^+ A549 cells is ~1.7x relative to GFP^- A549 cells (N=15, ±SEM). (C) Total MIIA overexpression in nucleofected MEG-01 cells is ~1.7x for GFP-WT and ~1.3x for GFP-D1424N mutant relative to GFP^- MEG-01 cells (N>25,000 events, ±SEM, *P<0.001). (D) Quantitation of A549 cells displaying myosin aggregates (N≥30, *P<0.05). (E) In A549 cells, exogenous myosin is seen to accumulate in aggregates compared to the surrounding cytoplasm while total myosin (exogenous + endogenous) is similarly present in both aggregates and cytoplasm (N≥65, ±SEM, *P<0.05). (F) Co-transfection of mCherry WT MIIA with either GFP WT or D1424N MIIA. Quantitation shows MIIA aggregation is driven by the introduction of D1424N MIIA (N≥7 cells, ±SEM). Representative micrographs for each transfection showing that GFP D1424N MIIA aggregates recruit mCherry WT MIIA (scale bar = 10 μm).

Supplemental Tables

Table S1. List of antibodies described in Methods

Experiment	Buffer	Antibody	Dye/ Conjugate	Time (min)/ Temp (°C)	Dilution	Manufacturer
Rheometry & PLP Generation	Tyrode's + PGE1 (1:1000)	-	7-AAD	60 / 20	1:1000	Sigma
		-	Hoescht 33342	60 / 37	1:2500	Invitrogen
		anti-hu CD41	APC	60 / 37	1:20	Biolegend
		pS1943 MIIA	-	120 / 20	1:100	Cell Signaling
		anti-hu MIIA	-	120 / 20	1:100	Cell Signaling
		donkey anti-rb	Alexa 488	60 / 20	1:400	Invitrogen
Functional Characterization of MEG-01 Derived PLPs	Tyrode's + PGE1 (1:1000) + Ca^{2+} (1mM)	-	7-AAD	60 / 20	1:1000	Sigma
		anti-hu CD41	APC	60 / 37	1:20	Biolegend
		Annexin V	PE	60 / 20	1:10	BD Biosciences
Micropipette Aspiration	1% BSA	-	Hoescht 33342	45 / 37	1:1000	Invitrogen
		anti-hu CD41	PE	45 / 37	1:10	eBioscience
Proplatelet Imaging	3% BSA + 0.05% Tween-20	pS1943 MIIA	-	4 / ~16	1:100	Cell Signaling
		anti-hu MIIA	-	4 / ~16	1:100	Cell Signaling
		anti-hu MIIB	-	4 / ~16	1:100	Sigma
		donkey anti-rb	Alexa 488	60 / 20	1:400	Invitrogen
		anti-hu CD41	APC	60 / 20	1:100	Biolegend
		-	Hoescht 33342	5 / 20	1:10000	Invitrogen
Proplatelet Flow Cytometry	Tyrode's	anti-hu CD41	APC	45 / 20	1:20	Biolegend
		Glycophorin A	PE	45 / 20	1:20	Biolegend
		-	Hoescht 33342	45 / 20	1:2500	Invitrogen

Supplemental Figure 1

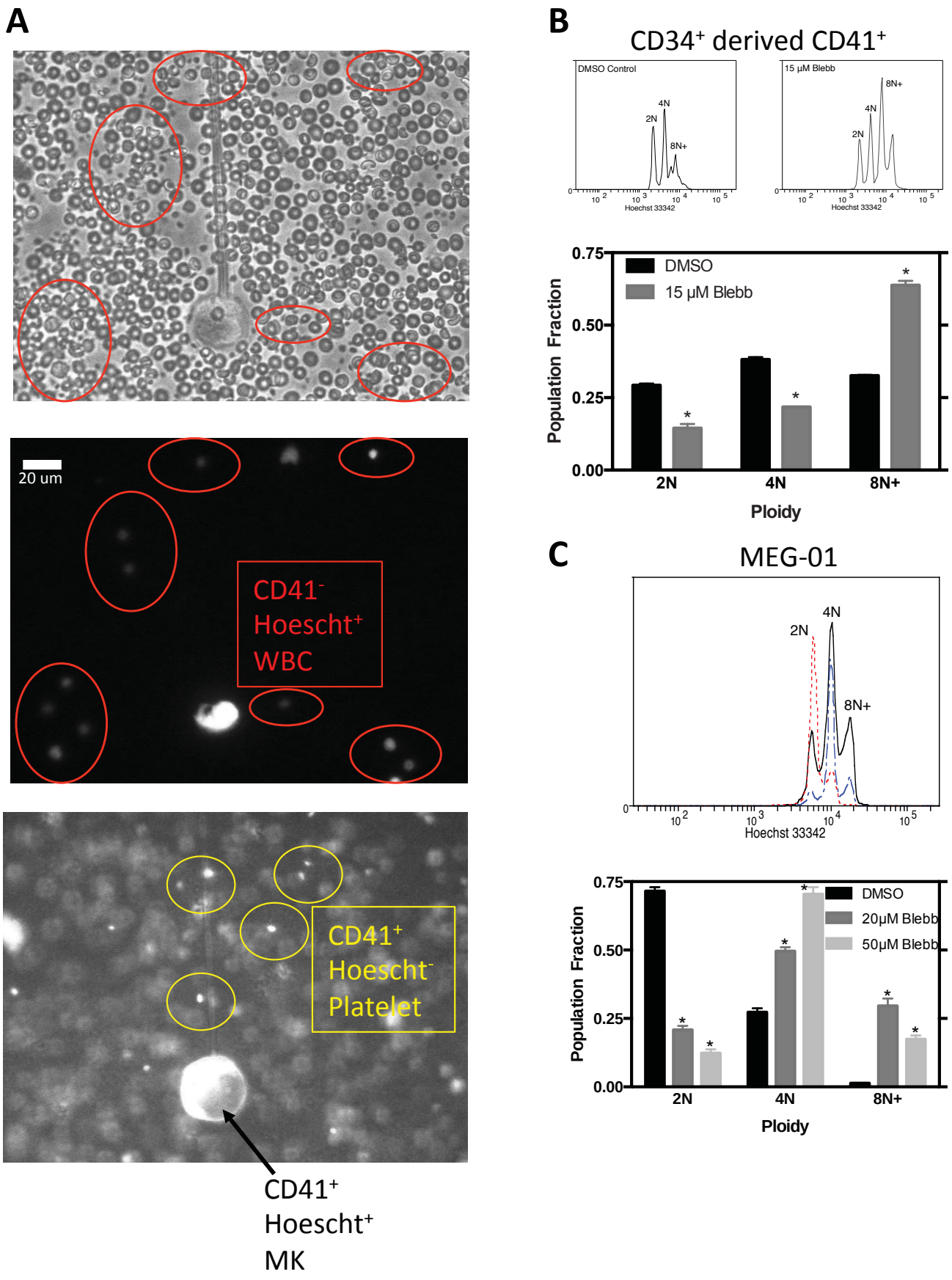

Supplemental Figure 2

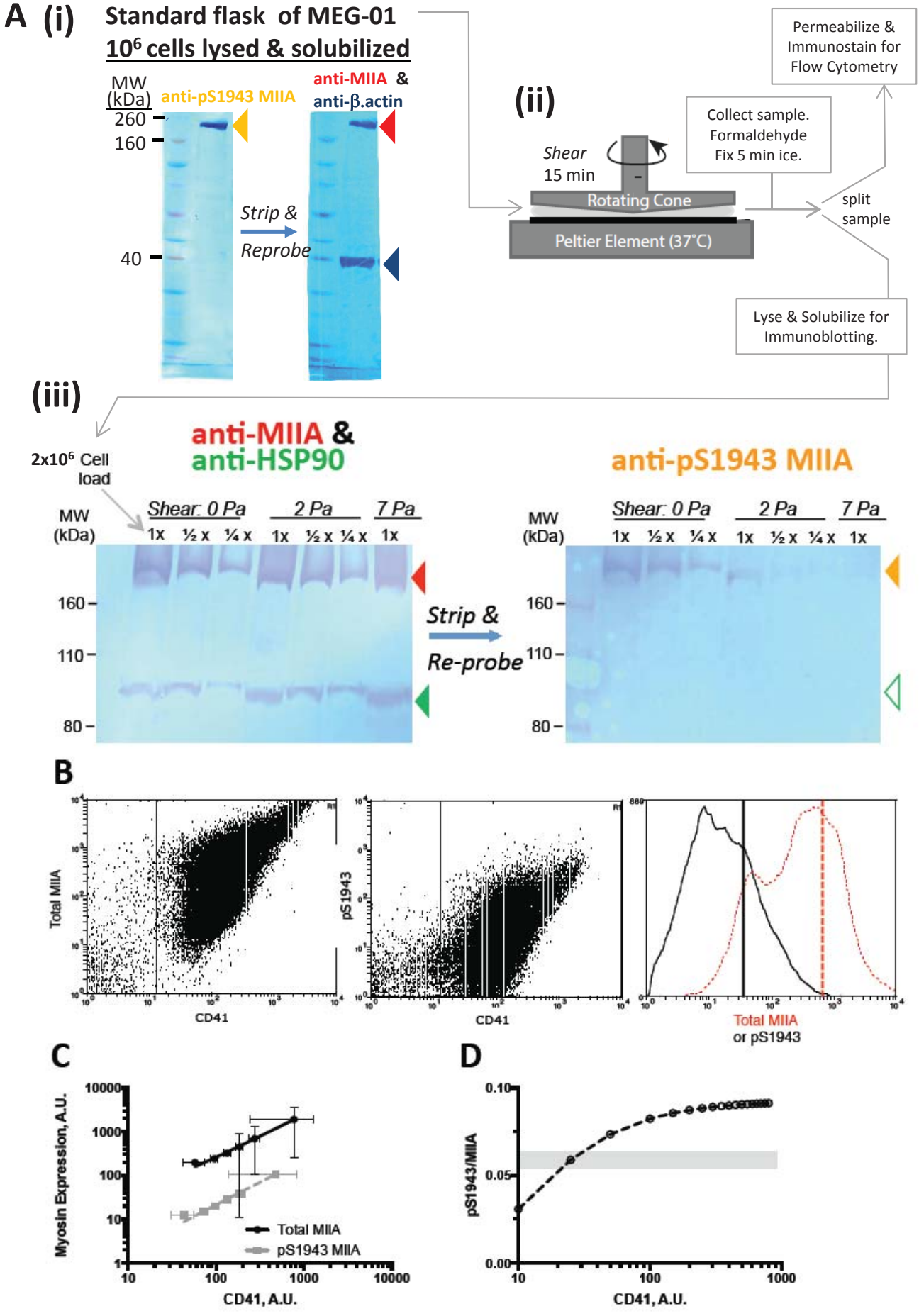

Supplemental Figure 3

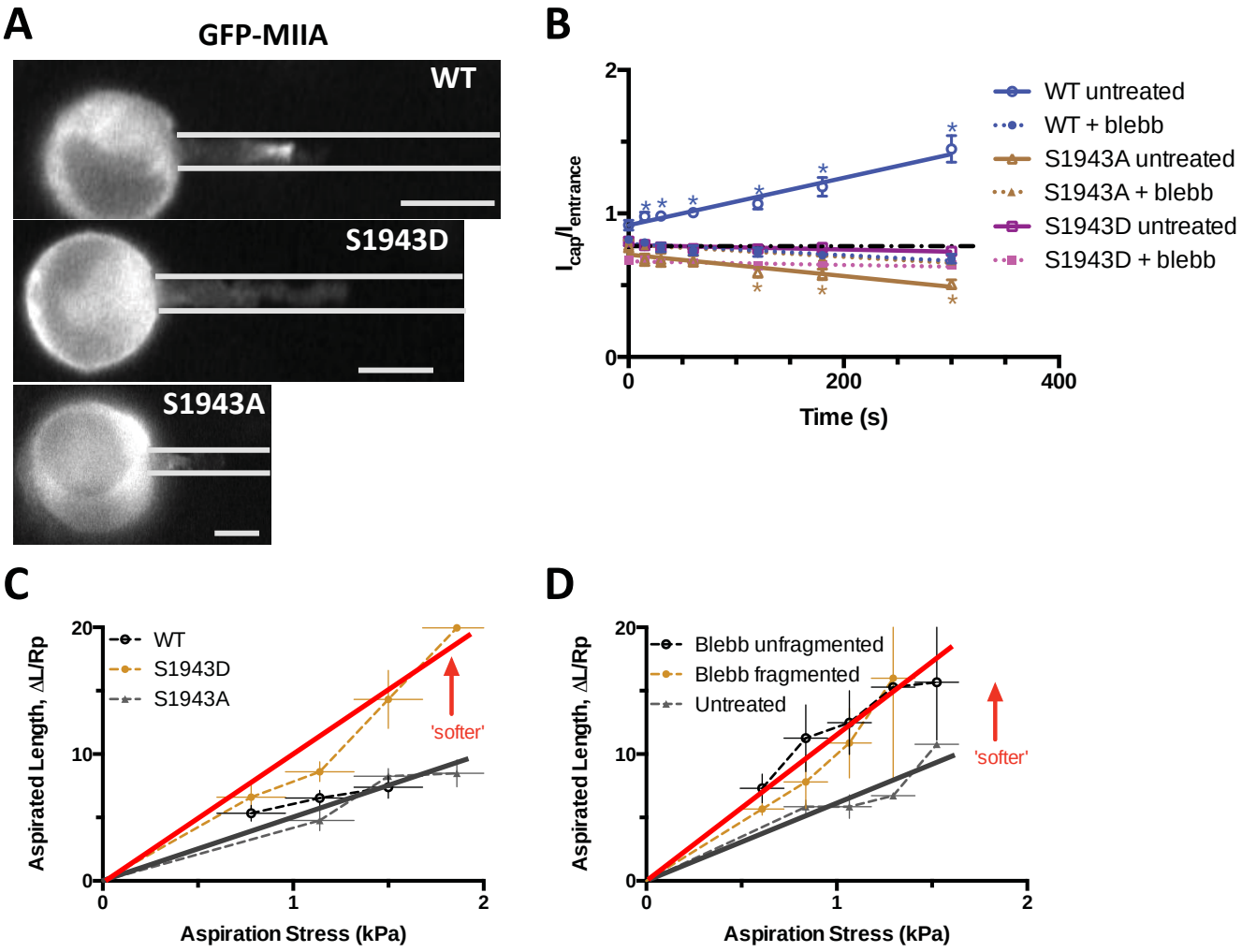

Supplemental Figure 4

A

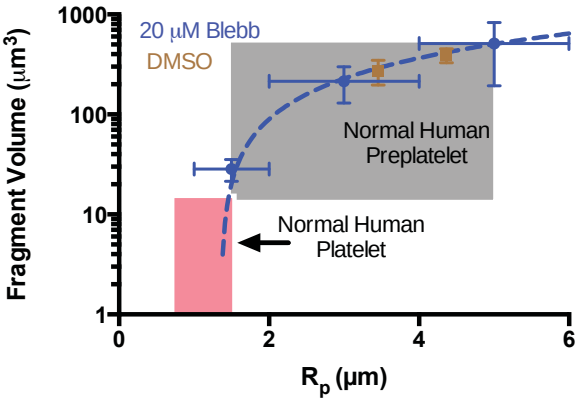

B

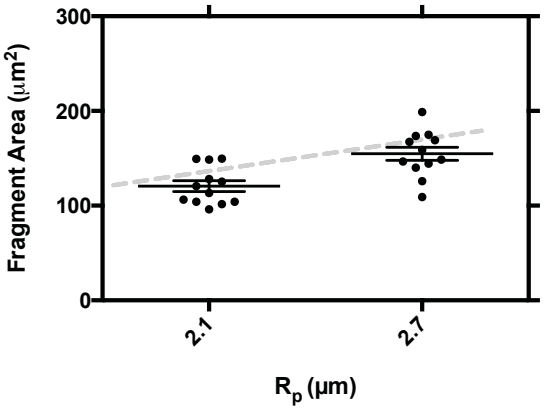

C

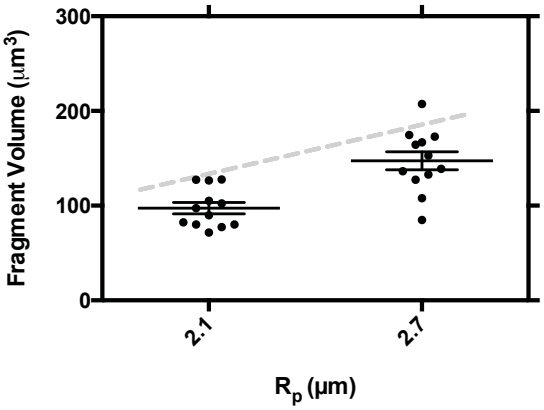

Supplemental Figure 5